

## ARTICLE



# Hedgehog blockade remodels the gut microbiota and the intestinal effector CD8<sup>+</sup> T cells in a mouse model of mammary carcinoma

Dominique C. Hinshaw<sup>1,8</sup>, Courtney A. Swain<sup>1,8</sup>, Dongquan Chen<sup>2,3,4</sup>, Ann Hanna<sup>5</sup>, Patrick A. Molina<sup>6</sup>, Craig L. Maynard<sup>1,6</sup>, Goo Lee<sup>1</sup>, Braden C. McFarland<sup>6</sup>, Rajeev S. Samant<sup>1,2,7</sup> and Lalita A. Shevde<sup>1,2</sup>✉

© The Author(s), under exclusive licence to United States and Canadian Academy of Pathology 2022

Given the gut microbiome's rise as a potential frontier in cancer pathogenesis and therapy, leveraging microbial analyses in the study of breast tumor progression and treatment could unveil novel interactions between commensal bacteria and disease outcomes. In breast cancer, the Hedgehog (Hh) signaling pathway is a potential target for treatment due to its aberrant activation leading to poorer prognoses and drug resistance. There are limited studies that have investigated the influences of orally administered cancer therapeutics, such as Vismodegib (a pharmacological, clinically used Hh inhibitor) on the gut microbiota. Using a 4T1 mammary carcinoma mouse model and 16 S rRNA sequencing, we longitudinally mapped alterations in immunomodulating gut microbes during mammary tumor development. Next, we identified changes in the abundance of commensal microbiota in response to Vismodegib treatment of 4T1 mammary tumor-bearing mice. In addition to remodeling gut microbiota, Vismodegib treatment elicited an increase in proliferative CD8<sup>+</sup> T cells in the colonic immune network, without any remarkable gastrointestinal-associated side effects. To our knowledge, this is the first study to assess longitudinal changes in the gut microbiome during mammary tumor development and progression. Our study also pioneers an investigation of the dynamic effects of an orally delivered Hh inhibitor on the gut microbiome and the gut-associated immune-regulatory adaptive effector CD8<sup>+</sup> T cells. These findings inform future comprehensive studies on the consortium of altered microbes that can impact potential systemic immunomodulatory roles of Vismodegib.

*Laboratory Investigation* (2022) 102:1236–1244; <https://doi.org/10.1038/s41374-022-00828-1>

## INTRODUCTION

The microbiota, a key regulator of inflammation, comprises many bacterial niches throughout the human body, such as the gut and oral cavity. The diversity in the environment of each organ system results in variation of the microbiota across these sites. Additionally, diet, genetics, chronic diseases, and other internal and external factors also impact the abundance of microbial populations.<sup>1,2</sup> The gastrointestinal microbiota has a profound impact on overall health and disease.<sup>3</sup> Importantly, polymorphic microbiomes are becoming an emerging cancer hallmark.<sup>4</sup> In addition to commensal microbes' association with cancer progression and treatment responsiveness, the various microbiomes of the human body can also release detectable metabolites that can be used as possible biomarkers to aid in cancer screening and precision medicine.<sup>5</sup> Beyond the role in unique digestive processes, the gut microbiome protects the gut from potential pathogenic bacteria, regulates immune processes, and produces key immunomodulatory metabolites.<sup>1,6–8</sup>

Dysbiosis, or the disruption to the microbiota homeostasis, has been associated with chronic inflammation in cancers including hepatocellular carcinoma and colorectal cancer.<sup>7,8</sup> In breast cancer, the gut and breast microbiota hold unique signatures dependent on prognostic stage and hormone-receptor status.<sup>9,10</sup> The nature of the gut microbiome has also been shown to modulate cancer treatment response of melanoma patients to anti-PD-1 immunotherapy.<sup>11</sup> The microbiome has been identified as a possible risk factor and has been linked to variable treatment response, such as tumor burden and drug tolerance, in breast cancer patients treated with chemotherapeutics or immunotherapeutics.<sup>12,13</sup> As such, the challenge of targeting specific microbes associated with tumorigenesis may provide a new perspective in breast cancer treatment.<sup>12–15</sup>

In addition to its roles in embryogenesis and in regulating tissue development, aberrant activation of the Hedgehog (Hh) pathway is associated with malignant progression and treatment resistance.<sup>16–19</sup> Its role in breast cancer is appreciated for programming

<sup>1</sup>Department of Pathology, University of Alabama at Birmingham, Birmingham, AL, USA. <sup>2</sup>O'Neal Comprehensive Cancer Center, University of Alabama at Birmingham, Birmingham, AL, USA. <sup>3</sup>Division of Preventive Medicine, Department of Medicine, University of Alabama at Birmingham, Birmingham, AL, USA. <sup>4</sup>Center for Clinical and Translational Sciences, University of Alabama at Birmingham, Birmingham, AL, USA. <sup>5</sup>Vanderbilt Center for Immunobiology, Vanderbilt University School of Medicine, Nashville, TN, USA. <sup>6</sup>Cell, Developmental, and Integrative Biology, University of Alabama at Birmingham, Birmingham, AL, USA. <sup>7</sup>Birmingham VA Medical Center, Birmingham, AL, USA. <sup>8</sup>These authors contributed equally: Dominique C. Hinshaw, Courtney A. Swain. ✉email: lsamant@uab.edu

Received: 6 May 2022 Revised: 1 July 2022 Accepted: 6 July 2022  
Published online: 30 July 2022

stemness attributes, metastasis, and drug resistance.<sup>16,17</sup> We have reported that Hh blockade promotes a pro-inflammatory TME through modifications of key immune populations in a 4T1 mammary mouse model, which included an increase in intratumoral cytotoxic CD8<sup>+</sup> T cells.<sup>20</sup> The Hh signaling cascade is initiated by the binding of a Hh-specific short-acting polypeptide ligand to Patched, a receptor that inhibits the regulatory molecule Smoothed (Smo). Upon ligand binding, the transmembrane protein, Smo, translocates to the primary cilium of the cell, activating intracellular signaling and leading to activation of the GLI transcription factors and consequently, activation of Hh target genes.<sup>19</sup> The Hh antagonist, Vismodegib, is effective in treating basal cell carcinoma and medulloblastoma, and is currently being used in clinical trials for combination therapies in breast cancer.<sup>16,21–23</sup>

In gastric cancer, *Helicobacter pylori* infection requires canonical Hh signaling to recruit immune cells involved in the metaplastic development of the gastric mucosa.<sup>22</sup> Not much is known about the influence of Hh signaling on the gut microbiome in cancers beyond the gastrointestinal tract. Past studies have highlighted prominent microbial taxa that can influence breast cancer development, progression, treatment, and staging in the context of immunotherapies and chemotherapies. Therefore, investigating microbial shifts caused by orally administered cancer therapeutics can reveal interactions of the host-microbiome axis that may influence treatment response. Since Vismodegib is an orally available FDA-approved Hh inhibitor, it is critical to understand how this inhibitor impacts the gut microbiome and how these microbial influences contribute to changes in the immunosurveillance mechanisms in the gut.

In this study, we adopted a longitudinal study utilizing a syngeneic, immunocompetent breast carcinoma mouse model to investigate the dynamic changes in the gut microbiome induced during mammary tumor development. Next, we proceeded to pharmacologically inhibit Hh signaling on the gut microbiome and assessed the impact of Hh blockade on microbial diversity. Our findings reveal that the gut microbiome is remodeled during syngeneic mammary tumor development characterized by alterations in the abundance and composition of bacterial species associated with tumorigenesis. Vismodegib (Smo-i) treatment led to further alterations in the gut microbiota and accompanying changes in the intestinal immune profile, characterized by proliferating CD8<sup>+</sup> T cells in the intraepithelial lymphocyte (IEL), lamina propria lymphocyte (LPL), and mesenteric lymph node (mLN) populations of the colon. Cumulatively, our results demonstrate that alteration of the gut microbiome, induced during tumor development, is further reformed by the orally administered Hh inhibitor.

## MATERIALS AND METHODS

### 4T1 mammary cancer mouse model

The animal procedures were completed with prior approval from the University of Alabama at Birmingham's Institutional Animal Care and Use Committee. Five-week-old female BALB/c immunocompetent mice were purchased from Jackson Laboratories (Farmington, CT) and maintained in non-germ-free conditions. We utilized 10 mice per treatment group that were treated longitudinally across two independent experiments (5 mice per treatment group, per experiment). After an acclimation period of 4 days,  $5 \times 10^5$  4T1 luciferase-expressing cells were injected orthotopically into the inguinal mammary fat pad under sterile conditions. Tumor growth was recorded through caliper measurements and through bioluminescent imaging (BLI). Once tumors reached 3 mm<sup>2</sup> in diameter, the mice were randomized into control or Smo-i treatment groups. On day 13, Smo-i (Vismodegib; Selleck Chemical, Houston, TX) or vehicle control (DMSO) was administered via oral gavage. All gavage needles were autoclaved prior to treatment administration. Mice were treated 3 times weekly for 3 weeks. Mice were fed the NIH-31 Open Formula mouse and rat standard diet throughout the study. For in vivo BLI, mice were intraperitoneally injected with 2.5 mg of D-luciferin, anesthetized by isoflurane inhalation, and

imaged after 10 minutes using an In Vivo Imaging System (IVIS)<sup>®</sup> 100 Xenogen (Perkin Elmer, Inc., USA).

### Sample collection

Fecal collection from mice was initiated after the acclimation period (before tumor cell injection), day 7 after injection of 4T1 cells, day 13 (week 1 of treatment), day 20 (week 2 of treatment), and day 27 (week 3 of treatment). Fecal pellets were collected from five mice per treatment group. Upon termination of the experiment, contents within the cecum of the mice were collected (day 40). Mammary tumors, colon tissue, cecum contents, mLNs, and lungs were also harvested at experiment endpoint. Colon weight and length was recorded. The gut microbiome profile was assessed at days 7, 13, and 27, which correspond to stages of 4T1 mammary tumor progression including very early tumor-bearing (TBV), early tumor-bearing (TBE), and late tumor-bearing (TBL) timepoints, respectively.

### 16 S sequencing

We sequenced the V4 region of the 16 S rRNA<sup>23</sup> that was accomplished using degenerate primers originally taken from Caparoso et al.<sup>24</sup> The UAB Microbiome Core modified the primers as described by Kumar et al.<sup>25</sup> for use on the Illumina MiSeq sequencer. PCR is carried out under conditions described by Kozich et al.<sup>26</sup> and Kumar et al.<sup>25</sup> PCR products were resolved on agarose gels and DNA was isolated and purified using Qiagen kits, which is then followed up quantification. The products are sequenced on the MiSeq platform, a single flowcell, single lane instrument that can generate approximately 9Gb of sequence data from our paired end 250 bp run.

### Microbiome analysis

DNA was extracted from the fecal pellets and cecum contents (ZYMO Research, Tustin, CA). 16 S rRNA sequencing was performed to map the microbiome profile for both the vehicle control and Smo-i groups. SILVA was used for taxonomy assignment. Amplicon sequence variants (ASVs) were filtered at abundance level <0.0005%. Operational taxonomic unit (OTU) sequences and abundance were clustered with 97% identity to help merge strain level differences and to minimize errors associated with the sequencing technology. The ASV tables are generated using these filtered sequences and rarified at the minimum sample depth. To determine OTU abundance differences between the control and Smo-i groups, the data was filtered based on microbes that were significantly altered by a fold change of two or more between these groups, and then cross referenced with the top 50 most abundant species identified by the dada2 analysis. Given the longitudinal nature of the study, we also assessed variability in the gut microbiota within and between individual subjects over time using  $\alpha$  (alpha) and  $\beta$  (beta) diversity measures. Shannon diversity index and observed OTUs were generated to assess  $\alpha$  diversity and the Bray-Curtis dissimilarity distance matrix was generated to assess  $\beta$  diversity. Two biological replicates of the microbiome analyses were completed. The R package *Mothur* was used for the ASV filtering and table generation, as well as for the  $\alpha$  and  $\beta$  diversity calculations. For data visualization, the R packages *ggplot2* and *vegan* were used.

### Immunohistochemistry

Sections from formalin-fixed, paraffin-embedded colon tissue were deparaffinized and rehydrated with xylene and a graded ethanol series. For hematoxylin and eosin (H&E) staining, slides were stained in filtered and modified Harris hematoxylin, washed with running tap water, and then differentiated in 1% acid alcohol. Slides were counterstained with eosin and dehydrated through a graded ethanol series and three changes of xylene, cover-slipped, and mounted with Cytoseal. For immunohistochemistry (IHC), slides were stained with either CD68 (1:50, Santa Cruz), or myeloperoxidase (MPO; 1:150, Invitrogen). Slides were counterstained with hematoxylin and dehydrated through a graded ethanol series and three changes of xylene, cover-slipped, and mounted with Cytoseal. For immunofluorescence (IF), heat-induced antigen retrieval was performed in citrate buffer at pH 6.0 and blocked in normal donkey and goat serum. Slides were stained with primary antibodies CD8 $\alpha$  (1:50; Invitrogen) diluted in 1X PBS + 5% BSA. After 1X PBS washes, slides were stained with secondary antibody donkey anti-rat Alexa Fluor 594 (1:300; ThermoFisher) diluted in 1X PBS + 5% BSA. Autofluorescence was quenched using the TrueView Autofluorescence Quenching Kit with DAPI (Vector Labs, Burlingame, CA) following the manufacturer's protocol and cover-slipped

for consequent analysis. Analysis was performed using a Nikon Eclipse Ti-U microscope and the NIS Elements software (Melville, NY).

### Pathology histological review

Histopathologic analysis of H&E-stained mouse colonic tissue was reviewed by a clinical pathologist (G.L.) by light microscopy. Mucosal integrity of the colon of both 4T1 vehicle control and Smo-i-treated mice was assessed. Mice were evaluated for cryptic injury, mucosal loss, and necrosis. For immune profiling of colonic tissues by IHC, a blind review of colonic tissue slides was conducted for quantification.

### IEL, LPL, and mLN isolation and flow cytometry analysis

The mLNs and colon were excised from 4T1 tumor-bearing mice at the termination of the experiment. For the mLNs, cells were passed through a 70  $\mu\text{m}$  cell strainer, and the single-cell suspension was counted using a TC20 Automated cell counter (BioRad, Hercules, CA). Cells were then stained with fixable viability dye (eFlour 450; Thermo Fisher) in PBS, followed by incubation with primary conjugated extracellular antibodies CD4 and CD8 $\alpha$  (Biolegend, San Diego, CA). Flow cytometry data was acquired using a BD LSRII Analyzer. Fluorescence minus one (FMO) and single-color controls were used. For IEL and LPL isolation, the large intestines were harvested and cleaned for processing. Intestines were cut segmentally and placed into cold H2 wash buffer. To remove the colonic epithelial cells and IELs, the tissue was incubated in stripping buffer and the IEL fraction was filtered through 70  $\mu\text{m}$  and 40  $\mu\text{m}$  filters. The colonic tissues were transferred and resuspended in warm H2 wash buffer. Tissue was further processed using total digest buffer (1 mg/mL collagenase type IV, 0.1 U/mL dispase II, 200  $\mu\text{g}/\text{mL}$  DNase type I). After dissociation, the single-cell suspension was resuspending in 37% isosmotic Percoll and centrifuged to enrich LPL and IEL fractions. For dead cell exclusion, cells were stained with Zombie NIR live-dead. Fc receptor blockade (TrueStain FcX plus and anti-CD16.2 Fc $\gamma$ RIV, Biolegend) and extracellular staining was performed. Spectral cytometry data was acquired on a Cytex Northern Lights full spectral cytometer (Fremont, CA). All flow cytometry analysis was done using FlowJo v10 software (Ashland, OR). The gating sequence for assessing intestinal CD8 $^+$  T cell populations included live cells, CD45 $^+$  > single cells > CD3 $^+$  > TCR $\beta^+$  > CD8 $\alpha^+$  > Ki-67 $^+$ . All antibodies are listed in Table S1.

### Enumeration of metastatic nodules

Lungs were harvested from DMSO- and Smo-i-treated 4T1 tumor-bearing mice at the termination of the experiment (day 40) and fixed in Bouin's solution. Metastatic nodules on the lung were counted by gross examination and imaged using a stereo microscope.

### Statistical analysis

Statistical analyses were performed using GraphPad Prism 8 software (La Jolla, CA). Graphical representations were constructed using RStudio version 4.0.0 (Boston, MA) or GraphPad Prism 8 software. The Shapiro-Wilk normality test was used to test the assumption of normal distribution for all the datasets. The mean metastatic nodule count data and flow analyses were analyzed using a two-tailed, unpaired *t*-test. Shannon diversity index and the observed OTU was analyzed using a one-way ANOVA followed by Tukey's multiple comparisons test. PERMANOVA analysis was performed based on the Bray-Curtis indexes after 9999 permutations. The linear discriminant analysis (LDA) effect size (LEfSe) of OTUs between the vehicle control and Smo-i groups were generated using the LEfSe method (online Galaxy version 1.0; ref. 15). For the LEfSe analysis, the factorial Kruskal-Wallis test between the groups was set to  $\alpha$  of 0.05 and the threshold on logarithmic LDA score for discriminative features was set to 2.0.

## RESULTS

### Progression of 4T1 tumor growth induces a unique gut microbiome

We were first interested in determining longitudinal changes in the gut microbiota during tumor development and progression in 4T1 tumor-bearing mice. Changes of the microbiome were observed across stages of 4T1 tumor progression that included naive (day 0), very early tumor-bearing (day 7), early tumor-bearing (day 13), or late tumor-bearing (day 27) mice (Fig. 1A). LEfSe analysis revealed the top altered species between the naive and late tumor-bearing groups

(LDA > 2,  $p < 0.05$ ; Fig. 1B). The  $\alpha$  diversity index is used to assess diversity within sample groups, while the  $\beta$  diversity reveals diversity between the samples. A heatmap of the Bray-Curtis dissimilarity matrix was constructed to visualize  $\beta$  diversity of the gut microbiota during tumor development (Fig. 1C). The naive samples are substantially dissimilar as compared to all samples through tumor development, illustrating modification of the gut microbiome during 4T1 tumor development and progression. We generated a list of the top 50 most abundant species when comparing naive and tumor-bearing mice using the dada2 platform and filtered the list to microbes that were changing by 2-fold or greater with a significant *p*-value ( $p > 0.05$ ). We narrowed down the results to six microbes that were found to be relevant to tumor development in other cancer models (Fig. 1D; refs. 27–29). While the abundance of *Ruminoclostridium* decreased in very early tumor-bearing mice (TBV), the levels remained steady at these decreased levels in early and late tumor-bearing mice (TBE and TBL, respectively). The abundance of *Clostridiales vadinBB60*, *Lactobacillus gasseri*, *Lachnospiraceae*, and *Anaeroplasma* decreased in TBV mice, and continued to decline longitudinally. In contrast, the abundance of *Muribaculaceae* increased in TBV mice and remained consistently increased in TBE and TBL mice. LEfSe analysis also revealed significantly altered bacterial species when comparing across the various tumor-bearing groups (Fig. S1A–E). These additional LDA analyses underscored the remarkable changes in species of the gut microbiota during 4T1 tumor progression.

### Hh inhibition alters the composition of the fecal and cecal microbiota in 4T1 mammary tumor-bearing mice

Smo-i is a pharmacological inhibitor of Hh activity.<sup>30</sup> Since Smo-i is orally administered, we conjectured that Smo-i might impact the gut microbiome of mammary tumor-bearing mice. To investigate this, we inoculated mice with luciferase expressing 4T1 mammary carcinoma cells. When the tumors were palpable (around 3 mm<sup>2</sup> in diameter), we randomized the 4T1 tumor-bearing mice for treatment with vehicle control or Smo-i. Fecal samples were collected across five time points, and cecum contents were collected upon experiment termination (Fig. 2A summarizes the experimental design). While tumor growth was comparable between the Smo-i and vehicle control groups (Fig. S2A–C), there was a significant decrease in the pulmonary metastatic nodules from 4T1 mice treated with Smo-i as compared to those administered vehicle control (Fig. 2B). We mapped changes in the gut microbiota in response to tumor progression and Smo-i in naive ( $n = 5$ ), very early tumor-bearing (non-treated,  $n = 20$ ), and tumor-bearing (vehicle control and Smo-i-treated across 3 collection time points at days 13, 20, and 27 post tumor injection,  $n = 30$  for each treatment group) mice. Significant alterations of the gut microbiome were observed at the phylum, family, and genus level (Fig. 2C–E). Naive mice possessed a prominent abundance of *Tenericutes*. The top phyla dominating the gut microbiome of the 4T1 tumor-bearing mice included *Firmicutes*, *Bacteroidetes*, *Verrucomicrobia*, *Tenericutes*, and *Proteobacteria*. Additionally, the OTU abundance at the family and genus level revealed considerable variations in both, the fecal and cecal microbiome, across the different treatment groups and timepoints (Fig. 2D, E). The common families found in all fecal and cecal samples included *Lachnospiraceae*, *Muribaculaceae*, *Lactobacillaceae*, *Akkermansiaceae*, and *Ruminococcaceae*. The common genera across the fecal and cecal samples included *Muribaculaceae*, *Lactobacillus*, *Lachnospiraceae*, *Akkermansia*, and *Bacteroidales*.

### Hh inhibition modifies the $\beta$ diversity of the gut microbiome

To analyze variations in the fecal and cecal microbiome between naive, DMSO, and Smo-i-treated mice,  $\alpha$  and  $\beta$  indexes were plotted and statistically analyzed. There were minor changes in the  $\alpha$  diversity indexes (Shannon diversity index and observed OTUs) in response to 4T1 tumor development and Smo-i treatment (Fig. 3A, B). However, there were significant differences



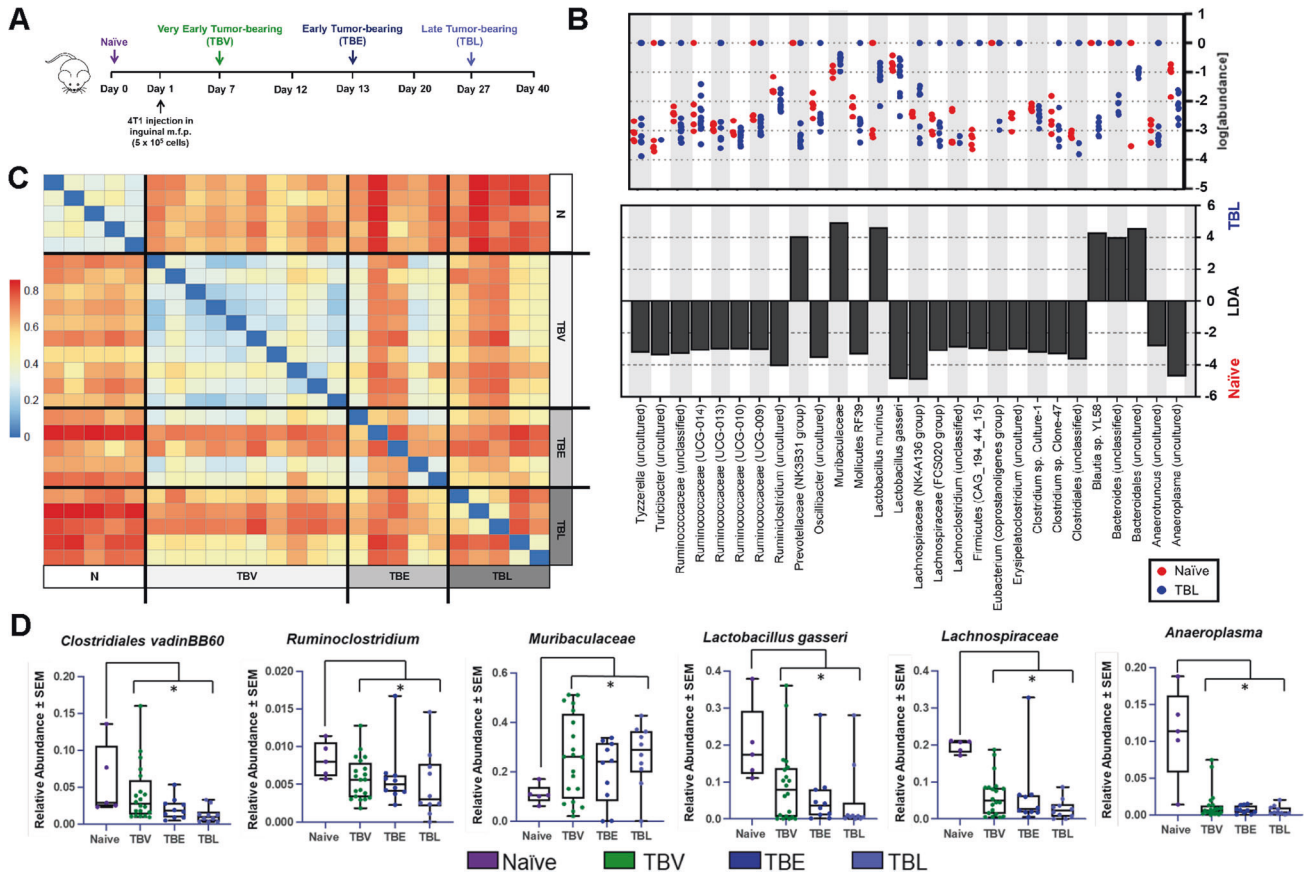


**Fig. 1** Progression of 4T1 mammary tumor development and progression induces changes within the fecal microbiome. **A** Schematic of the designated stages and timepoints for 4T1 tumor development. **B** LefSe (effect size) analysis results comparing naive with late tumor-bearing at the species level (bottom) alongside the abundance of the species (top). Each symbol represents an individual sample. **C** Heatmap representing Bray-Curtis dissimilarity matrix of fecal samples from N, TBV, TBE, and TBL mice. **D** Bar plots of the fold change of relevant top species found to be significantly altered between the naive and tumor-bearing samples. Error bars represent  $\pm$  SEM. N naive; TBV very early tumor-bearing; TBE early tumor-bearing; TBL late tumor-bearing; \* $p < 0.05$ .

in the  $\beta$  diversity of the fecal samples between DMSO and Smo-i-treated groups throughout tumor progression, as represented in the NMDS plot, Bray-Curtis dissimilarity matrix heatmap, and the principle of coordinate analysis (PCA; Fig. 3C–E). Significant differences were determined by PERMANOVA using the comparison of the Bray-Curtis  $\beta$ -diversity indexes between the DMSO and Smo-i-treated fecal samples ( $p = 0.026$ ; Fig. 3F). As such, the DMSO and the Smo-i-treated groups were divergent with respect to their microbiome profile.

#### Hh inhibition modulates the abundance bacteria involved in systemic immunomodulation

To study the effects of Hh inhibition on the gut microbiome of the 4T1 mouse model, microbes that were significantly altered by a fold change of two or more between the fecal samples of DMSO and Smo-i-treated groups were filtered. Various bacterial species with immunomodulating roles in cancer were significantly altered in Smo-i-treated mice, as assessed by LefSe (Fig. 4A). The *Firmicutes*:*Bacteroidetes* ratio was calculated to inform dysbiosis in the gut microbiome (Fig. 4B). Broadly comparing vehicle versus Smo-i-treated mice, the *Firmicutes*:*Bacteroidetes* ratio was significantly decreased in Smo-i-treated mice. Further, with disease progression, while the *Firmicutes*:*Bacteroidetes* ratio decreased, the separation between the DMSO and the Smo-i-treated group was evident, with the ratio of the Smo-i group being significantly lower than the control group. Fecal and cecal OTUs of top altered bacterial species were compared between the DMSO and Smo-i groups (Fig. 4C, D). Mapping these immunomodulating fecal bacteria longitudinally

revealed similar trends with respect to changes in abundance throughout tumor progression and response to Smo-i treatment (Fig. 4E). Interestingly, the *Ruminococcaceae* and *Lachnospiraceae* families are positively correlated with Treg abundance in acute graft-versus-host-disease.<sup>31</sup> Moreover, *L. murinus* is associated with the induction of immunosuppressive Tregs in calorie restricted mice.<sup>32</sup> LefSe analysis revealed significantly altered microbes at the phyla, class, order, family, and genus levels between the DMSO and Smo-i-treated groups in both fecal and cecal samples (Fig. 53A, B). Overall, we find that treatment of mice with Smo-i diminishes the abundance of microbes that can potentially contribute to systemic immune responses within and beyond the gut.

#### Hh inhibition increased proliferating CD8<sup>+</sup> T cells across the immune network in the colon

Commensal gut microbes interact with key immune cell populations such as cytotoxic CD8<sup>+</sup> T cells.<sup>33</sup> This interaction has been implicated to be a mechanism by which the gut microbiome can influence anti-tumor immunity at distal sites.<sup>33,34</sup> Therefore, we assessed the intestinal CD8<sup>+</sup> T cell populations residing in the IEL and LPL fractions of the colonic epithelium, as well as those residing in the mLNs of DMSO and Smo-i-treated tumor-bearing mice. For IEL and LPL flow analysis, colon tissue was excised and digested before proceeding to live/dead staining, Fc block, and extracellular staining. Focused analyses of the IEL and LPL conventional (TCR $\alpha\beta$ <sup>+</sup>) CD8<sup>+</sup> T cells were performed using the gating strategy outlined in Fig. 54. Although there were no major changes in overall CD45<sup>+</sup> lymphocyte, CD3<sup>+</sup> T cell, and CD8<sup>+</sup> T

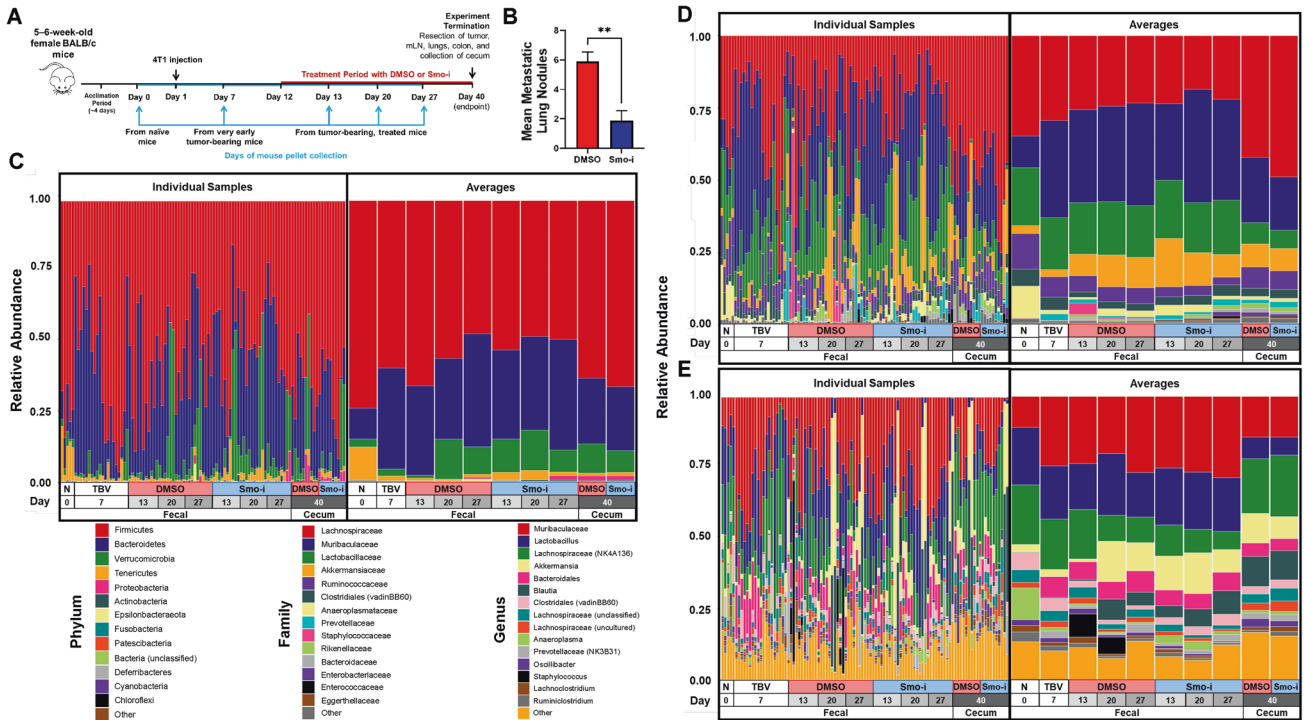


**Fig. 2** Hh inhibition impacts the gut bacterial abundance in the 4T1 immunocompetent model of mouse mammary carcinoma. **A** Schematic of the experimental design for the 4T1 mouse model. **B** Mean metastatic lung nodules from DMSO ( $n = 8$ ) and Smo-i-treated ( $n = 7$ ) mice. Error bars represent  $\pm$  SEM. **C** Stacked bar plots of the relative abundance of common bacterial taxa at the phylum level, **D** the family level, and **E** the genus level of the fecal ( $n = 85$ ) and cecal ( $n = 20$ ) microbiome of naive, very early (non-treated) tumor-bearing, and tumor-bearing mice treated with DMSO or Smo-i. N, naive; TBV, very early tumor-bearing; TB, tumor-bearing. \*\*\* $p < 0.001$ .

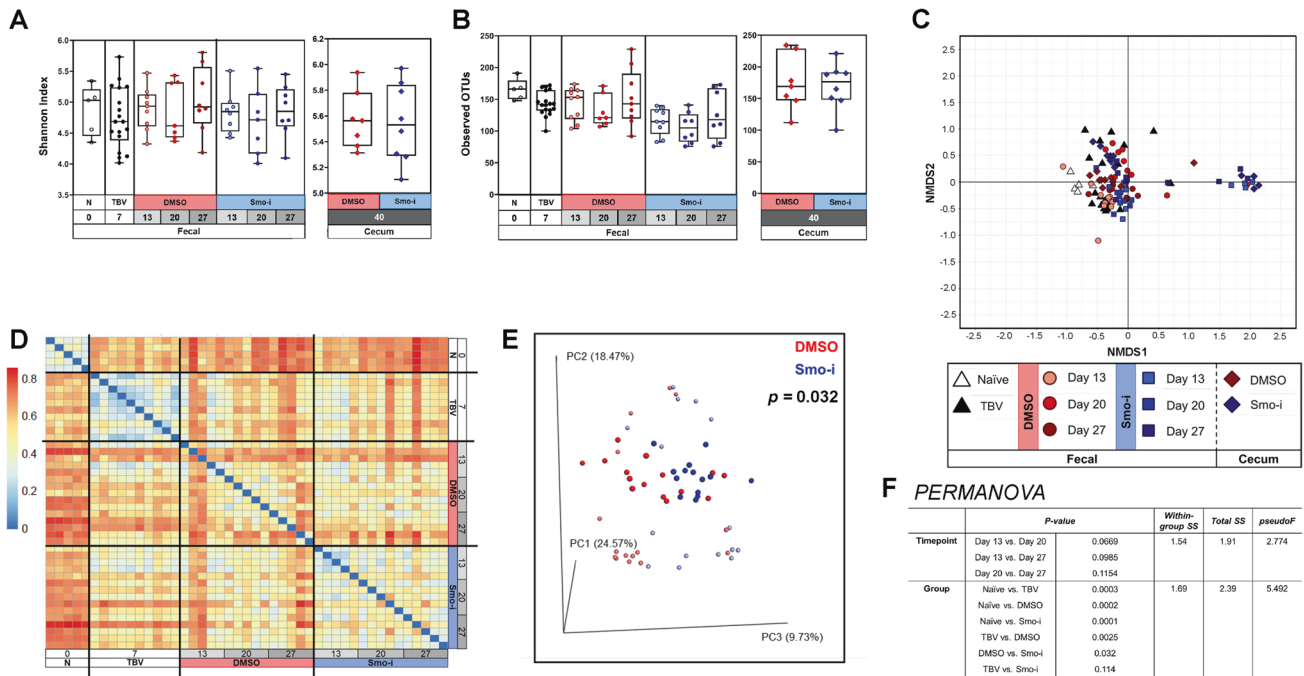


**Fig. 3** Hh inhibition alters the  $\alpha$  and  $\beta$  diversity of the fecal and cecal microbiota. **A** Shannon diversity index and **B** observed OTUs of the fecal and cecal microbiota of naive, very early tumor-bearing (non-treated), vehicle control, and Smo-i-treated 4T1 mice are shown to represent  $\alpha$  diversity. Symbols represent individual mice, and the box-and-whisker plots represent the minimum and maximum values. **C** NMDS plot of Bray-Curtis indices of the fecal (triangles, circles, and squares) and cecal (diamonds) microbiota between groups with a stress value of 0.2. **D** Heatmap representing the Bray-Curtis dissimilarity matrix between fecal samples ( $n = 45$ ). The  $\beta$  diversity is illustrated by a heatmap of Bray-Curtis dissimilarity distances. **E** A principal coordinate analysis of fecal and cecal samples ( $n = 105$ ) by treatment group using Bray-Curtis distances. Dark red and dark blue representing DMSO and Smo-i treatment from experiment 1, and light blue and light red representing DMSO and Smo-i treatment from experiment 2. **F** Summary of PERMANOVA analysis with  $p$  and  $pseudof$  values between vehicle control and Smo-i groups, as well as between timepoints. \*\* $p < 0.01$ , \* $p < 0.05$ .

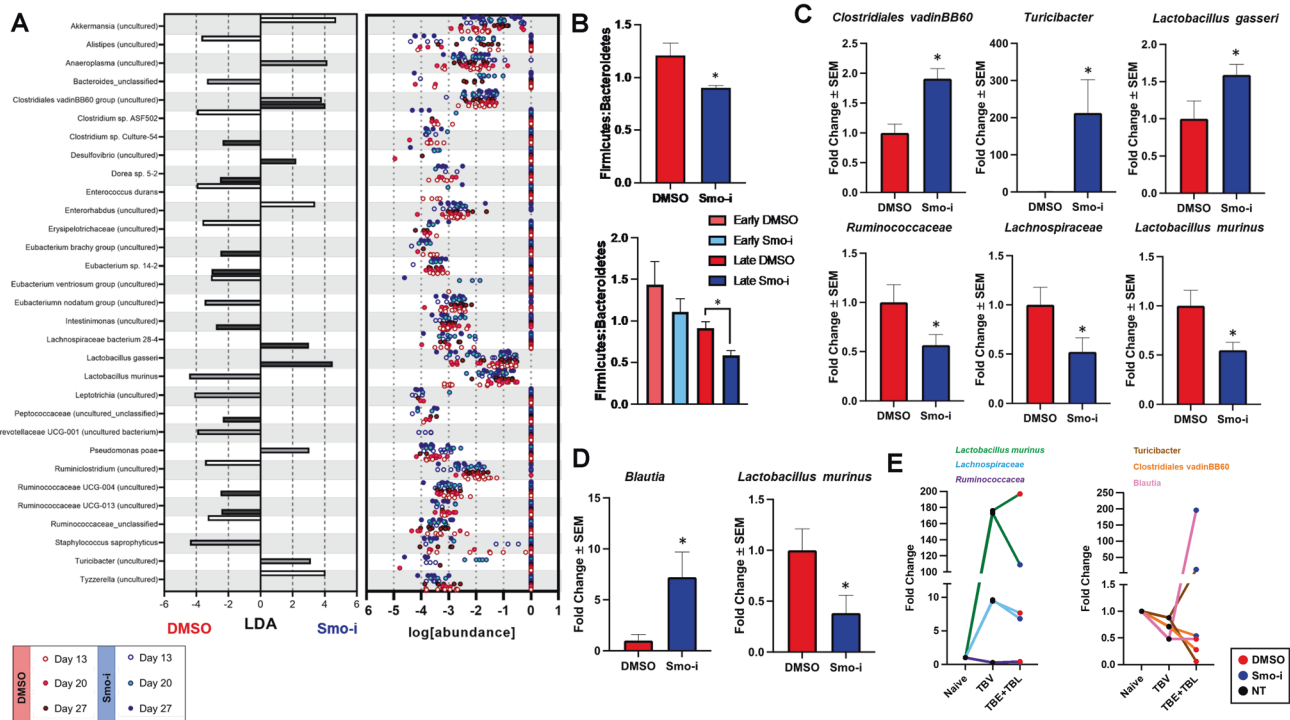


**Fig. 4** Hh blockade progressively modifies the gut microbiota in mammary tumor-bearing mice. **A** LefSe analysis comparison between DMSO and Smo-i groups at each timepoint (day 13, 20, 27) at the species level (left) alongside the abundance of the given species (right). Each symbol represents an individual sample. **B** *Firmicutes*:*Bacteroidetes* ratios comparing DMSO and Smo-i (top) and further stratified by early vs late DMSO and Smo-i-treated 4T1 mice ( $n = 30$  per group) in fecal samples. **C** Bar plots of the fold change of species and genera with greatest change in abundance between DMSO and Smo-i-treated 4T1 mice ( $n = 30$  per group) in fecal samples. **D** Bar plots of the fold change of top bacterial species and genera between DMSO and Smo-i-treated 4T1 mice ( $n = 10$  per group) in cecum samples. **E** Line plots of the fold change of bacterial species found to have similar trends in overall abundance changes throughout tumor development of DMSO and Smo-i-treated mice. Error bars represent  $\pm$  SEM.  $*p < 0.05$ .

cell populations, there was a significant increase in the abundance of the proliferative CD8<sup>+</sup> T cell population (evident by Ki-67 expression) in Smo-i-treated mice (Fig. 5A). These findings were also seen in the LPL CD8<sup>+</sup> T cell population (Fig. 5B). To determine if these changes extended to secondary lymphoid organs proximal to the colon, we analyzed the CD8<sup>+</sup> T cell population of the mLNs. The mLNs were excised and processed into a single cell suspension for flow cytometry analysis. The analysis revealed an increase in CD8<sup>+</sup> T cell population in the Smo-i-treated mice (Fig. 5C). To visualize these changes in the CD8<sup>+</sup> T cell populations we stained the colon tissue of Smo-i-treated and vehicle control tumor-bearing mice. We registered an increase in the population of CD8<sup>+</sup> T cells in the colon of Smo-i-treated mice, as compared to control (Figs. 5D and S5A). However, there were no notable changes in colonic innate immune populations neutrophils and macrophages, as assessed by IHC staining for MPO and CD68 respectively (Fig. S5B). In summary, these data suggest that Smo-i-induced changes to the microbiome are associated with proliferation of resident CD8<sup>+</sup> T cells in the colon and mLNs.

#### Hh inhibition does not cause drug-induced colitis in 4T1 tumor bearing mice

Given the results of the intestinal CD8<sup>+</sup> T cell analysis, we wanted to confirm that these changes were not due to Smo-i-induced intestinal injury. Cryptic damage and loss observed in the colon tissue from Smo-i-treated 4T1 mice was comparable to colon tissue from vehicle control mice (Fig. 6A). Drug-induced gastrointestinal damage is a growing concern for cancer patients receiving chemotherapy and could also be a confounding variable in the CD8<sup>+</sup> T cell analysis if colitis is present.<sup>35</sup> Therefore, we were interested in discovering any potential toxicity of Smo-i on the gastrointestinal tract. Given that the

shortening and edema of the colon are common symptoms of colitis, we used colon weight and length as measures for colitis.<sup>36</sup> There were no significant differences between the Smo-i and vehicle control mice in these measures. Conclusively, the proliferation of intestinal CD8<sup>+</sup> T cells in Smo-i-treated mice was not a result of drug-induced colonic injury or colitis.

#### DISCUSSION

There is growing evidence that the gut microbiome is modified during breast cancer tumorigenesis and progression. Moreover, the microbiome is becoming recognized as an influential factor of therapeutic responsiveness in cancer treatment. We utilized a 4T1 syngeneic mouse model to better understand the dynamics in the microbial composition of the gut during mammary tumorigenesis and to observe the changes induced by oral administration of Smo-i. By employing 16 S rRNA gene sequencing of fecal and cecal samples from naive and tumor-bearing mice we identified notable shifts in the abundance of bacterial species that are linked to tumor progression. Oral administration of Smo-i further restructured the gut microbiota accompanied by remarkable changes in the abundance of proliferating CD8<sup>+</sup> T cells across the intestinal immune network.

The two dominant bacterial phyla in the human gut include *Bacteroidetes* and *Firmicutes*,<sup>37</sup> and these phyla make up a large majority of the gut microbiota in our naive and 4T1 tumor-bearing mice. The 4T1 tumor-bearing mice had a prominent expansion of bacteria within the *Bacteroidetes* phylum in the gut microbiome as compared to the naive mice. Substantial changes in the *Firmicutes*:*Bacteroidetes* ratio have been shown in some studies to be representative of dysbiosis in the gut microbiome and have been regarded as a biomarker for several pathologies such as obesity,



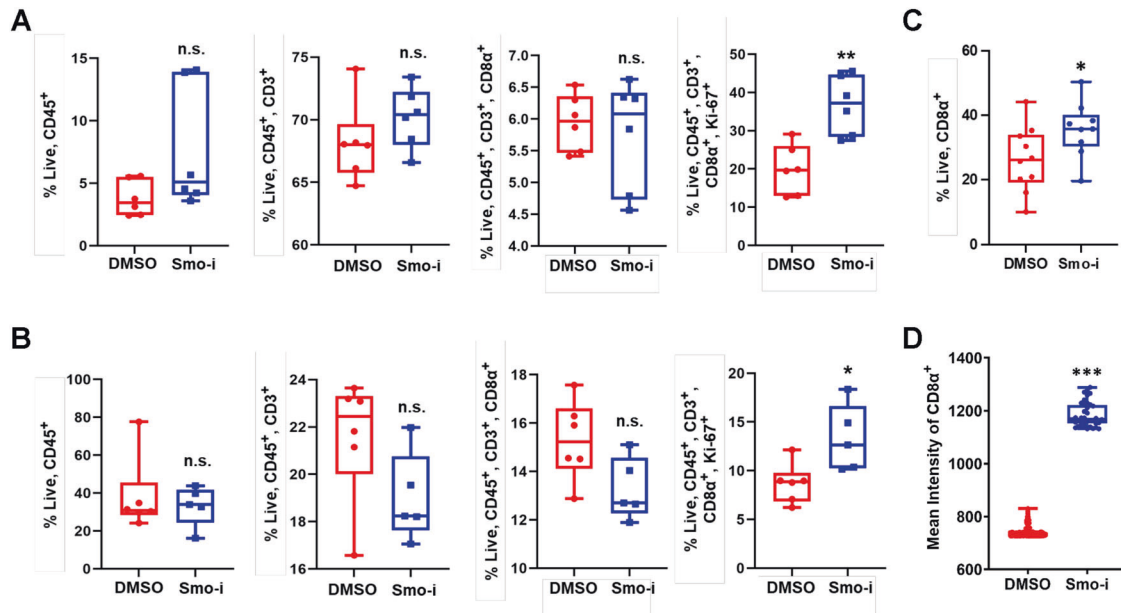


**Fig. 5** Smo-i treatment augments the proliferation of CD8<sup>+</sup> T cells in the colon and the mesenteric lymph nodes. **A** Flow cytometry was used to assess the abundance and proliferation of conventional CD8<sup>+</sup> T cell populations as well as their proliferative status (as assessed by Ki-67 expression) from IELs and **B** LPLs isolated from vehicle control and Smo-i-treated mice. **C** The mLNs of vehicle control and Smo-i-treated tumor-bearing mice were excised and analyzed through flow cytometry. The abundance of CD8<sup>+</sup> T cells was observed. Each point represents an individual sample for all flow analyses. **D** Colonic tissue from vehicle control and Smo-i-treated tumor-bearing mice were stained with DAPI (blue) and CD8 $\alpha$  (red) by secondary (indirect) IF. Graph represents mean intensity of CD8 $\alpha$ <sup>+</sup>. Each point represents an object of intensity determined by the NIS Elements software. Error bars represents minimum/maximum values. \* $p < 0.05$ , \*\* $p < 0.005$ , \*\*\* $p < 0.001$ .

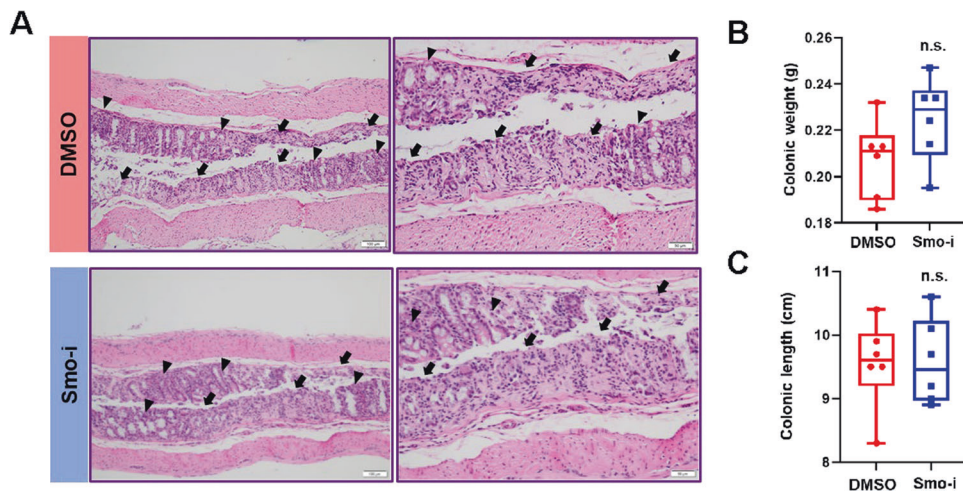


**Fig. 6** The oral administration of Smo-i does not induce colitis in 4T1 tumor-bearing mice. **A** Representative H&E images of mouse colon tissue from DMSO-treated (top) and Smo-i-treated (bottom) tumor-bearing mice at 10X (left) and 20X (right). Arrows represent areas of crypt loss and arrow heads denote adjacent remaining crypts for reference. Scale bars represent 100  $\mu$ m (left) or 50  $\mu$ m (right) as indicated. **B** Colonic weight and **C** length recorded from vehicle control and Smo-i-treated mice.

cardiovascular diseases, type 2 diabetes, and cancer, although the use of this ratio as a biomarker remains controversial.<sup>37–39</sup> Bacterial species that correlate with an unfavorable microbiome within the gut are commonly linked to the *Bacteroidetes* phylum. For example, *Bacteroides fragilis*, a common colonizer of the gut, is capable of oncogenic transformation through the production of a virulent zinc metalloprotease toxin, the *B. fragilis* toxin.<sup>40,41</sup> Additionally, enterotoxigenic *B. fragilis* has been found to have a direct effect on promoting breast carcinogenesis when colonized in the gut or breast duct.<sup>9</sup> In contrast, colonic bacteria within the phylum *Firmicutes* have been found to be highly abundant in healthy patients and are reduced during colorectal cancer progression.<sup>42</sup> We registered a

significant decrease in the *Firmicutes*:*Bacteroidetes* ratio in mice that were administered Smo-i.

Beyond the phyla level, various bacteria of the gut can contribute to systemic immunity through interactions with key immune populations involved in anti-tumor immunity. For example, bacterial strains in the *Lactobacillus* genus have been linked to immunomodulation within and beyond the gut.<sup>43,44</sup> *Lactobacillus reuteri* have been shown to induce anti-inflammatory regulatory T cells (Tregs) in many studies.<sup>39,40</sup> Through adenosine A<sub>2A</sub> receptors, *Lactobacillus reuteri* is solely capable of remodeling the gut microbiota and suppressing autoimmunity in response to Treg depletion.<sup>44</sup> Select *Lactobacillus gasseri* strains have been

shown to augment antioxidant activity and to protect colonic mucosa against colorectal neoplasia through various mechanisms including the suppression of pro-inflammatory signals.<sup>45</sup> In calorie-restricted mice, *Lactobacillus murinus* could attenuate the potent anti-inflammatory nature of the gut microbiota and induce the immunosuppressive phenotype of Tregs.<sup>46</sup> Aligning nicely with these reports, our results revealed a reduction in the protective species, *Lactobacillus gasseri*, during mammary tumor development and an increase in response to Smo-i treatment. We also registered a reduction in the Treg-promoting species, *Lactobacillus murinus*, in response to Smo-i treatment.

The gut microbiota of Smo-i treated mice demonstrated altered abundance of bacteria associated with *Lachnospiraceae* and *Ruminococcaceae*. The families, *Lachnospiraceae* and *Ruminococcaceae*, consist of butyrate-producing bacteria. Microbial-derived butyrate has been classified as a metabolite that is associated with reduced tumorigenesis.<sup>28</sup> In a microbiome study of multiple sclerosis patients, there was a positive correlation between the abundance of *Lachnospiraceae* and both, the differentiation of Tregs and the stimulation of TGF- $\beta$  and IL-10 production by monocytes.<sup>47</sup> *Anaeroplasm* has also been identified as TGF- $\beta$ - and IgA-inducing bacteria. This microbe induces TGF- $\beta$  expression in follicular helper T cells in Peyer's patches and promotes mucosal IgA-related immune responses and production.<sup>27</sup> Species belonging to the *Clostridia* clusters XIVa and IV have been associated with the immunosuppressive activity and promotion of infiltrating Tregs in colon tissue,<sup>48</sup> while *Turicibacter* is implicated in inflammation through TNF expression.<sup>49</sup> As such, there is immense reshaping of the gut microbiota in response to oral administration of Smo-i.

Commensal microbes that interact with immune populations can modulate anti-tumor immunity and cancer immunotherapy response through the augmented activation of tumor-infiltrating cells, especially CD8<sup>+</sup> T cells.<sup>6,33,50–53</sup> Therefore, changes in this key immune population are informative of the presence of gut microbes capable of interacting with other host immune cells and stimulating proliferative signaling in the colonic epithelium.<sup>51–53</sup> Furthermore, microbes are capable of being translocated from the gut to peripheral lymph nodes via immune cells as part of intestinal inflammation.<sup>44</sup> Tanoue et al.<sup>53</sup> noted an association of CD8<sup>+</sup> T cell infiltration and microbiota-mediated activation in the colon in response to specific commensal bacteria. Smo-i enhanced the proliferative activity of colonic CD8<sup>+</sup> T cells. IEL and LPL CD8<sup>+</sup> T cell populations are lymphocytes specialized in providing significant protection of the mucosal barrier and integrity of the epithelial surface.<sup>50</sup> Despite the proliferation of intestinal CD8<sup>+</sup> T cells, histological review of the colon of mice in our study revealed that Smo-i did not induce more extensive colonic injury or colitis as compared to vehicle control. The enhanced proliferative status of CD8<sup>+</sup> T cells in the gut of 4T1 mice in response to Smo-i treatment suggests that the bacterial species altered by Smo-i may be capable of influencing key immune cell populations. There is growing evidence indicating that the gut microbiome and its associated metabolites (i.e., SCFAs and lipopolysaccharides) can influence host immunity and TME at distal sites. Furthermore, microbial SCFAs can travel systemically.<sup>56</sup> The SCFAs pentanoate and butyrate, were found to enhance the anti-tumor immunity of cytotoxic T cells and chimeric antigen receptor T cells epigenetically and metabolically in syngeneic melanoma and pancreatic cancer mouse models.<sup>6</sup> Thus, targeting commensal microbes involved in priming or expanding key immune cells of anti-tumor immunity would be a compelling venture in further interpreting this microbiome-host crosstalk in the context of Smo-i.

Our study pioneers a longitudinal perspective of the shifts in the abundance of the gut microbiome during mammary tumor progression. These findings also showcase a novel discovery of the effects of orally administered Smo-i on modifying the gut

microbiome. Given the gut microbiome's rise as a potential frontier in cancer pathogenesis and therapy, leveraging microbial analyses in the study of breast tumor progression and treatment is essential in unveiling interactions between commensal bacteria and the TME. Various studies that investigate the gut microbiome in both human and mouse models have associated specific bacterial species within cohorts of treatment-responsive subjects to be involved in inducing favorable immune responses. The gut microbiome has an extended role in shaping systemic immune responses and responsiveness to immunotherapy.<sup>4,5,54,55</sup> Therefore, optimizing new approaches to implementing microbial analyses in the clinic can lead to a better understanding of treatment resistance. Further studies are required to determine the functional repertoire of the microbes found to be altered in response to treatment with Smo-i. Future comprehensive studies on the consortium of altered microbes and their associated metabolites are necessary to characterize their potential systemic immunomodulatory roles.

## DATA AVAILABILITY

The datasets used and/or analyzed in this study are available from the corresponding author upon reasonable request.

## REFERENCES

1. Maynard C, Elson C, Hatton R, & Weaver C. Reciprocal interactions of the intestinal microbiota and immune system. *Nature* 489, 231–241 (2012).
2. Lozupone C, Stombaugh J, Gordon J, Jansson J & Knight R. Diversity, stability and resilience of the human gut microbiota. *Nature* 489, 220–230 (2012).
3. Schwabe R & Jobin C. The microbiome and cancer. *Nature Reviews Cancer* 13, 800–812 (2013).
4. Hanahan D. Hallmarks of Cancer: New Dimensions. *Cancer Discovery* 12, 31–46 (2022).
5. Cullin N, Azevedo Antunes C, Straussman R, Stein-Thoeringer C, & Elinav E. Microbiome and cancer. *Cancer Cell* 39, 1317–1341 (2021).
6. Luu M, Riestler Z, Baldrich A, Reichardt N, Yuille S, Buseti A et al. Microbial short-chain fatty acids modulate CD8<sup>+</sup> T cell responses and improve adoptive immunotherapy for cancer. *Nature Communications* 12, 4077 (2021).
7. Francescone R, Hou V & Grivennikov SI. Microbiome, Inflammation, and Cancer. *The Cancer Journal* 20 (2014).
8. Grivennikov SI, Greten FR & Karin M. Immunity, Inflammation, and Cancer. *Cell* 140, 883–899 (2010).
9. Banerjee S, Tian T, Wei Z, Shih N, Feldman MD, Peck KN et al. Distinct Microbial Signatures Associated With Different Breast Cancer Types. *Frontiers in Microbiology* 9, 951 (2018).
10. Luu TH, Michel C, Bard J-M, Dravet F, Nazih H & Bobin-Dubigeon C. Intestinal Proportion of *Blautia* sp. is Associated with Clinical Stage and Histoprognostic Grade in Patients with Early-Stage Breast Cancer. *Nutrition and Cancer* 69, 267–275 (2017).
11. Gopalakrishnan V, Spencer CN, Nezi L, Reuben A, Andrews MC, Karpinetz TV et al. Gut microbiome modulates response to anti-PD-1 immunotherapy in melanoma patients. *Science* 359, 97–103 (2018).
12. Armstrong H, Bording-Jorgensen M, Dijk S & Wine E. The Complex Interplay between Chronic Inflammation, the Microbiome, and Cancer: Understanding Disease Progression and What We Can Do to Prevent It. *Cancers* 10 (2018).
13. Parida S, Wu S, Siddharth S, Wang G, Muniraj N, Nagalingam A et al. A Pro-carcinogenic Colon Microbe Promotes Breast Tumorigenesis and Metastatic Progression and Concomitantly Activates Notch and  $\beta$ -Catenin Axes. *Cancer Discovery* 11, 1138 (2021).
14. Bhateja P, Cherian MM, Majumder S & Ramaswamy B. The Hedgehog Signaling Pathway: A Viable Target in Breast Cancer? *Cancers* 11 (2019).
15. Segata N, Izard J, Waldron L, Gevers D, Miropolsky L, Garrett WS et al. Metagenomic biomarker discovery and explanation. *Genome Biology* 12, R60 (2011).
16. Amakye D, Jagani Z & Dorsch M. Unraveling the therapeutic potential of the Hedgehog pathway in cancer. *Nature Medicine* 19, 1410–1422 (2013).
17. Hui M, Cazet A, Nair R, Watkins DN, O'Toole SA & Swarbrick A. The Hedgehog signalling pathway in breast development, carcinogenesis and cancer therapy. *Breast Cancer Research* 15, 203 (2013).
18. Eggenschwiler JT & Anderson KV. Cilia and Developmental Signaling. *Annual Review of Cell and Developmental Biology* 23, 345–373 (2007).
19. Rubin LL & de Sauvage FJ. Targeting the Hedgehog pathway in cancer. *Nature Reviews Drug Discovery* 5, 1026–1033 (2006).



20. Hanna A, Metge BJ, Bailey SK, Chen D, Chandrashekar DS, Varambally S et al. Inhibition of Hedgehog signaling reprograms the dysfunctional immune micro-environment in breast cancer. *Oncoimmunology* 8, 1548241 (2019).
21. National Library of Medicine (U.S.). Addition of Vismodegib to Neoadjuvant Chemotherapy in Triple Negative Breast Cancer Patients (SHH-CM). Identifier NCT02694224 (2016).
22. Merchant JL & Ding L. Hedgehog Signaling Links Chronic Inflammation to Gastric Cancer Precursor Lesions. *Cellular and Molecular Gastroenterology and Hepatology* 3, 201-210 (2017).
23. Woese CR & Gutell RR. Evidence for several higher order structural elements in ribosomal RNA. *Proc Natl Acad Sci USA* 86, 3119-3122 (1989).
24. Caporaso JG, Lauber CL, Walters WA, Berg-Lyons D, Lozupone CA, Turnbaugh PJ et al. Global patterns of 16S rRNA diversity at a depth of millions of sequences per sample. *Proceedings of the National Academy of Sciences* 108, 4516-4522 (2011).
25. Kumar R, Eipers P, Little RB, Crowley M, Crossman DK, Lefkowitz EJ et al. Getting started with microbiome analysis: sample acquisition to bioinformatics. *Curr Protoc Hum Genet* 82, 18.18.11-29 (2014).
26. Kozich JJ, Westcott SL, Baxter NT, Highlander SK & Schloss PD. Development of a dual-index sequencing strategy and curation pipeline for analyzing amplicon sequence data on the MiSeq Illumina sequencing platform. *Appl Environ Microbiol* 79, 5112-5120 (2013).
27. Beller A, Kruglov A, Durek P, von Goetze V, Werner K, Heinz GA et al. Specific microbiota enhances intestinal IgA levels by inducing TGF- $\beta$  in T follicular helper cells of Peyer's patches in mice. *European Journal of Immunology* 50, 783-794 (2020).
28. Fong W, Li Q & Yu J. Gut microbiota modulation: a novel strategy for prevention and treatment of colorectal cancer. *Oncogene* 39, 4925-4943 (2020).
29. Miyake S, Kim S, Suda W, Oshima K, Nakamura M, Matsuoka T et al. Dysbiosis in the Gut Microbiota of Patients with Multiple Sclerosis, with a Striking Depletion of Species Belonging to Clostridia XIVa and IV Clusters. *PLOS ONE* 10, e0137429 (2015).
30. Zito PM, Nassereddin A, & Scharf R. Vismodegib. In: StatPearls [Internet]. Treasure Island (FL): Vismodegib. StatPearls Publishing (2022).
31. Han L, Jin H, Zhou L, Zhang X, Fan Z, Dai M et al. Intestinal Microbiota at Engraftment Influence Acute Graft-Versus-Host Disease via the Treg/Th17 Balance in Allo-HSCT Recipients. *Front Immunol* 9 (2018).
32. He B, Hoang TK, Wang T, Ferris M, Taylor CM, Tian X et al. Resetting microbiota by *Lactobacillus reuteri* inhibits T reg deficiency-induced autoimmunity via adenosine A2A receptors. *J Exp Med* 214, 107-123 (2017).
33. Spranger S, Spaapen RM, Zha Y, Williams J, Meng Y, Ha TT et al. Up-Regulation of PD-L1, IDO, and Tregs in the Melanoma Tumor Microenvironment Is Driven by CD8+ T Cells. *Science Translational Medicine* 5, 200ra116-200ra116 (2013).
34. Sivan A, Corrales L, Hubert N, Williams JB, Aquino-Michaels K, Earley ZM et al. Commensal *Bifidobacterium* promotes antitumor immunity and facilitates anti-PD-L1 efficacy. *Science* 350, 1084-1089 (2015).
35. Escalante J, McQuade RM, Stojanovska V & Nurgali K. Impact of chemotherapy on gastrointestinal functions and the enteric nervous system. *Maturitas* 105, 23-29 (2017).
36. Song JL, Choi JH, Seo JH, Lim YI & Park KY. Anti-Colitic Effects of Kanjangs (Fermented Soy Sauce and Sesame Sauce) in Dextran Sulfate Sodium-Induced Colitis in Mice. *Journal of Medicinal Food* 17, 1027-1035 (2014).
37. Magne F, Gotteland M, Gauthier L, Zazueta A, Pesoa S, Navarrete P et al. The Firmicutes/Bacteroidetes Ratio: A Relevant Marker of Gut Dysbiosis in Obese Patients? *Nutrients* 12, 1474 (2020).
38. Aguirre M & Venema K. Does the Gut Microbiota Contribute to Obesity? Going beyond the Gut Feeling. *Microorganisms* 3, 213-235 (2015).
39. Mell B, Jala VR, Mathew AV, Byun J, Waghulde H, Zhang Y et al. Evidence for a link between gut microbiota and hypertension in the Dahl rat. *Physiol Genomics* 47, 187-197 (2015).
40. Sears CL. The toxins of *Bacteroides fragilis*. *Toxicol* 39, 1737-1746 (2001).
41. Sears CL & Pardoll DM. Perspective: Alpha-Bugs, Their Microbial Partners, and the Link to Colon Cancer. *The Journal of Infectious Diseases* 203, 306-311 (2011).
42. Lu Y, Chen J, Zheng J, Hu G, Wang J, Huang C et al. Mucosal adherent bacterial dysbiosis in patients with colorectal adenomas. *Sci Rep* 6, 26337-26337 (2016).
43. Wells JM. Immunomodulatory mechanisms of lactobacilli. *Microbial Cell Factories* 10, S17 (2011).
44. Liu Y, Fatheree NY, Dingle BM, Tran DQ & Rhoads JM. *Lactobacillus reuteri* DSM 17938 Changes the Frequency of Foxp3+ Regulatory T Cells in the Intestine and Mesenteric Lymph Node in Experimental Necrotizing Enterocolitis. *PLOS ONE* 8, e56547 (2013).
45. Oh NS, Lee JY, Kim Y-T, Kim SH & Lee J-H. Cancer-protective effect of a synbiotic combination between *Lactobacillus gasseri* 505 and a *Cudrania tricuspidata* leaf extract on colitis-associated colorectal cancer. *Gut Microbes* 12, 1785803 (2020).
46. Pan F, Zhang L, Li M, Hu Y, Zeng B, Yuan H et al. Predominant gut *Lactobacillus murinus* strain mediates anti-inflammatory effects in calorie-restricted mice. *Microbiome* 6, 54-54 (2018).
47. Saresella M, Mendozzi L, Rossi V, Mazzali F, Piancone F, LaRosa F et al. Immunological and Clinical Effect of Diet Modulation of the Gut Microbiome in Multiple Sclerosis Patients: A Pilot Study. *Front Immunol* 8, 1391-1391 (2017).
48. Atarashi K, Tanoue T, Shima T, Imaoka A, Kuwahara T, Momose Y et al. Induction of Colonic Regulatory T Cells by Indigenous *Clostridium* Species. *Science* 331, 337-341 (2011).
49. Jones-Hall YL, Kozik A & Nakatsu C. Ablation of Tumor Necrosis Factor Is Associated with Decreased Inflammation and Alterations of the Microbiota in a Mouse Model of Inflammatory Bowel Disease. *PLOS ONE* 10, e0119441 (2015).
50. Konjar S, Ferreira C, Blankenhaus B & Veldhoen M. Intestinal Barrier Interactions with Specialized CD8 T Cells. *Front Immunol* 8 (2017).
51. Dzutsev A, Badger JH, Perez-Chanona E, Roy S, Salcedo R, Smith CK et al. Microbes and Cancer. *Annu Rev Immunol* 35, 199-228 (2017).
52. Luu M, Pautz S, Kohl V, Singh R, Romero R, Lucas S et al. The short-chain fatty acid pentanoate suppresses autoimmunity by modulating the metabolic-epigenetic crosstalk in lymphocytes. *Nature Communications* 10, 760 (2019).
53. Tanoue T, Morita S, Plichta DR, Skelly AN, Suda W, Sugiura Y et al. A defined commensal consortium elicits CD8 T cells and anti-cancer immunity. *Nature* 565, 600-605 (2019).
54. Heshiki Y, Vazquez-Urbe R, Li J, Ni Y, Quainoo S, Imamovic L et al. Predictable modulation of cancer treatment outcomes by the gut microbiota. *Microbiome* 8, 28 (2020).
55. De Oliveira GLV. Chapter 33 - The Gut Microbiome in Autoimmune Diseases. In: Joel Faintuch & Salomao Faintuch (eds). *Microbiome and Metabolome in Diagnosis, Therapy, and other Strategic Applications*. Academic Press 332 (2019).

## ACKNOWLEDGEMENTS

The authors acknowledge funding from the following sources: Department of Defense (W81XWH-14-1-0516, W81XWH-18-1-0036, W81XWH-10-1-0755) and O'Neal Invests awarded to L.A.S. The work is supported in part by BXAI3374 (VA) and CA194048 (NCI/NIH) to R.S.S. The authors acknowledge funding provided by T32AI007051-42 (awarded to D.C.H.) and 2T32GM8361-29 (awarded to C.A.S.). The authors thank Sarah Kammerud and Brandon Metge for editorial suggestions. The authors would like to thank the UAB Comprehensive Flow Cytometry Core supported by NIH Grants P30 AR048311 and P30 AI027667 and the UAB Comprehensive Cancer Center's Preclinical Imaging Shared Facility supported by NIH Grants P30 CA013148 and 1S1 OOD021697.

## AUTHOR CONTRIBUTIONS

All authors have read and approved the manuscript. D.C.H., A.H., C.A.S., C.L.M., P.A.M., and L.A.S. contributed to experimental design. D.C.H., A.H., C.A.S., C.L.M., P.A.M. were responsible for acquisition of data. D.C.H., C.A.S., D.C., C.L.M., P.A.M., G.L., B.C.M., R.S.S., and L.A.S. performed analysis and interpretation of data. C.A.S., D.C.H., A.H., R.S.S., D.C., C.L.M., P.A.S., G.L., B.C.M., and L.A.S. were involved in writing and revision of the manuscript.

## COMPETING INTERESTS

The authors declare no competing interests.

## ADDITIONAL INFORMATION

**Supplementary information** The online version contains supplementary material available at <https://doi.org/10.1038/s41374-022-00828-1>.

**Correspondence** and requests for materials should be addressed to Lalita A. Shevde.

**Reprints and permission information** is available at <http://www.nature.com/reprints>

**Publisher's note** Springer Nature remains neutral with regard to jurisdictional claims in published maps and institutional affiliations.

Springer Nature or its licensor holds exclusive rights to this article under a publishing agreement with the author(s) or other rightsholder(s); author self-archiving of the accepted manuscript version of this article is solely governed by the terms of such publishing agreement and applicable law.